Environmental Science & Technology

pubs.acs.org/est

Article

Isotope Data Constrains Redox Chemistry of Atmospheric Mercury

Zhengcheng Song, Shaojian Huang, Peng Zhang, Tengfei Yuan, and Yanxu Zhang*

Cite This: https://doi.org/10.1021/acs.est.4c02600

Read Online

ACCESS | Metrics & More | Article Recommendations | Supporting Information

ABSTRACT: The redox chemistry of mercury (Hg) in the atmosphere exerts a significant influence on its global cycle. However, our understanding of this important process remains shrouded in uncertainty. In this study, we utilize three-dimensional atmospheric Hg isotope modeling to evaluate the isotopic composition of particle-bound mercury [$Hg^{II}(P)$] in the global atmosphere. We investigate various chemistry mechanisms and find that they induce remarkably disparate odd-number mass-independent fractionation (odd-MIF) in $Hg^{II}(P)$ on a global scale. The observed odd-MIF data identify the essential role of sea salt aerosol debromination in the redox chemistry of atmospheric Hg and underscore the predominant influence of Br oxidation in the marine boundary layer. The odd-MIF signatures significantly narrow the uncertainty range of redox chemistry rates and constrain the photoreduction of $Hg^{II}(P)$ at a magnitude of 10^{-3} JNO_2 (local photolysis frequency of NO_2) in the global atmosphere. This study advances our understanding of atmospheric Hg chemistry processes and provides insights into the potential impacts of climate change on Hg cycling.

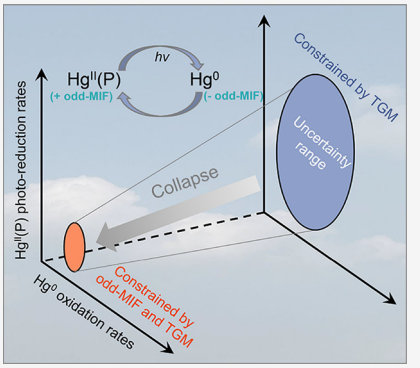

KEYWORDS: *atmosphere mercury chemistry, mercury isotope, isotope model, particle-bound mercury, GEOS-Chem*

1. INTRODUCTION

Mercury (Hg), a potent neurotoxin,[1−3] exists in three forms in the atmosphere: gaseous elemental (Hg^0), gaseous oxidized [$Hg^{II}(g)$], and particulate bound [$Hg^{II}(P)$].[4,5] Hg^0 can persist in the atmosphere for several months to a year and can be transported globally through atmospheric circulation.[6,7] However, it undergoes oxidation to $Hg^{II}(g)$ by oxidants like bromine (Br), chlorine (Cl), hydroxyl radicals (OH), and ozone (O_3), and is subsequently absorbed onto particles, forming $Hg^{II}(P)$.[8,9] Both $Hg^{II}(g)$ and $Hg^{II}(P)$ can be reduced back to Hg^0 or efficiently removed through wet and dry deposition, resulting in an atmospheric residence time of several days to weeks.[10,11] The redox chemistry thus has a significant impact on the global cycle of atmospheric Hg as it influences its forms, transportation, and deposition worldwide. Nevertheless, the precise details of these processes remain uncertain.

Global modeling studies have summarized the development of our understanding of atmospheric Hg chemistry.[11−15] Among them, Holmes et al.[6] suggested that the global-scale oxidation of Hg^0 is primarily initiated by Br radicals, along with a photoreduction process of Hg^{II} to Hg^0 within cloud droplets. Horowitz et al.[9] upgraded the mechanism that includes a two-stage oxidation process: Hg + Br → HgBr followed by HgBr + NO_2/HO_2 → Hg^{II}. Shah et al.[8] accommodated recent laboratory[11,13,14] and computational data and revealed both Br and OH are the main oxidants for the first stage, with subsequent oxidation initiated by O_3 and radicals in the second stage. However, there are two major knowledge gaps in Hg redox chemistry that hinder our complete understanding of the global Hg cycle. The first gap revolves around the abundance of atmospheric Br radicals, which subjects to a high degree of uncertainty and depends on the sea salt aerosol (SSA) debromination process in the marine boundary layer (MBL).[16,17] The second gap pertains to the photoreduction rate of $Hg^{II}(P)$, for which direct observations are lacking but is often adjusted to align with observed atmospheric Hg levels. It is typically scaled using the local photolysis frequency of NO_2 (JNO_2), and various models exhibit significant variations in scale factors.[6,8,9] These model studies, which employ different Br concentration fields and assume various photoreduction rates of $Hg^{II}(P)$, have yielded significant divergent atmospheric Hg budgets, even though they are all capable of reproducing observed atmospheric Hg concentrations and wet deposition fluxes. Indeed, additional constraints are required to disentangle atmospheric Hg chemistry mechanisms in the atmosphere.

Recent developments in Hg stable isotope techniques offer new avenues to address this issue. Mercury has seven isotopes that undergo mass-dependent fractionation (MDF, reported as $\delta^{202}Hg$) and mass-independent fractionation (MIF). MIF includes odd- (odd-MIF, reported as $\Delta^{199}Hg$ and $\Delta^{201}Hg$) and even-mass-number isotope MIF (even-MIF, reported as

Received: March 13, 2024
Revised: May 11, 2024
Accepted: May 16, 2024

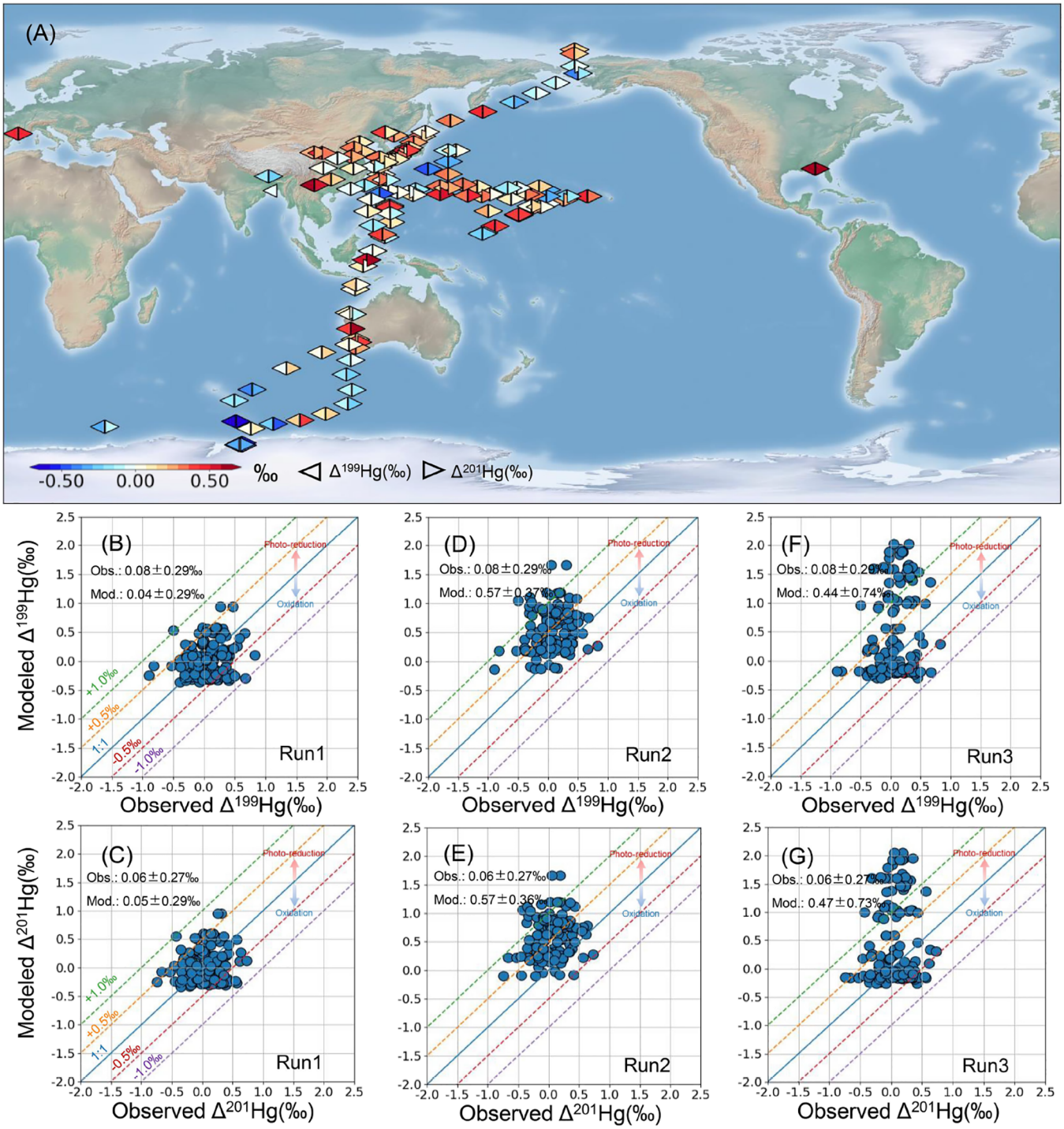

Figure 1. Synthesis of observations and simulations in odd-MIF of $Hg^{II}(P)$ in the globe.[4,20,26−29,31,60−64,67−75] (A) Global map marked with available observations for $\Delta^{199}Hg$ and $\Delta^{201}Hg$ of $Hg^{II}(P)$ samples (B−G) Comparison of simulations (annual mean) with measurements for $\Delta^{199}Hg^{II}(P)$ and $\Delta^{201}Hg^{II}(P)$ in the global atmosphere. In the figure, the arrows indicate that the photoreduction process can shift the $\Delta^{199}Hg^{II}(P)$ and $\Delta^{201}Hg^{II}(P)$ toward positive values, while the oxidation process has the opposite effect.

$\Delta^{200}Hg$ and $\Delta^{204}Hg$).[18,19] MDF is observed in almost all physical, chemical, and biological processes, while even-MIF is known to occur exclusively in photochemical reactions at free troposphere and/or tropopause.[20,21] Particularly, significant odd-MIF predominantly occurs in certain Hg photochemical transformations, such as the reduction of Hg^{II} and the oxidation of atmospheric Hg^0.[22−25] Mercury stable isotopes thus have the potential to trace the chemical processes of atmospheric Hg. The isotope signatures of $Hg^{II}(P)$, formed by redox chemistry, can reflect the information on redox processes, as demonstrated by the field studies conducted in urban, rural, and MBL regions.[4,26−32] While these studies have provided insights into atmospheric Hg chemistry, they are limited in space and time and cannot fully capture the heterogeneity of the global atmosphere.

In this study, we employ a global three-dimensional atmospheric Hg isotope model (GEOS-Chem-Hg-Isotope) to establish a link between atmospheric Hg chemistry and Hg

https://doi.org/10.1021/acs.est.4c02600
Environ. Sci. Technol. XXXX, XXX, XXX−XXX

Table 1. Hg Isotope Enrichment Factors of Odd-MIF in the Physical and Chemical Processes Contained in the Model[a]

no.	process	$E^{199}Hg$	$E^{201}Hg$	references
1	$Hg^0 + Br \rightarrow Hg^IBr$[b]	−0.23 ± 0.10‰	−0.14 ± 0.10‰	Sun et al.[24]
2	$Hg^0 + Cl \rightarrow Hg^ICl$[b]	−0.37 ± 0.10‰	−0.20 ± 0.10‰	Sun et al.[24]
3	$Hg^0 + OH \rightarrow Hg^IOH$[b]	−0.18 ± 0.10‰	−0.18 ± 0.10‰	Sun et al.[47]
4	$Hg^IY + O3 \rightarrow Hg^{II}(g)$[b] (Y = Cl/Br/OH)	−0.12 ± 0.10‰	−0.11 ± 0.10‰	Sun et al.[47]
5	$Hg^IY + BrO \rightarrow Hg^{II}(g)$[b] (Y = Cl/Br/OH)	1.01 ± 0.10‰	0.95 ± 0.10‰	Sun et al.[47]
6	$Hg^{II}(P)$+ hv(M) → Hg^0[c]	−2.75 ± 0.14‰	−2.75 ± 0.14‰	Sun et al.[43] Zheng and Hintelmann[22,23]
7	Hg^0 emission from soil[d]	eq 1	eq 2	Zhu et al.[49]
8	Hg^0 re-emission from land[e]	1.02 ± 0.02‰	1.02 ± 0.02‰	Sun et al.[43]
9	Hg^{II} photoreduction in snow[f]	1.40‰	1.40‰	assumed from Sherman et al.[50]
10	Hg^{II} photoreduction in ocean[g]	−0.15‰	−0.15‰	assumed from Zhao et al.[51] and Zhang et al.[52]

[a]The enrichment factors (E) are defined as the ratio of product to reactant. Reaction 5 exhibits positive enrichment factors distinct from other oxidation reactions. This disparity arises from the reversed magnetic isotope effect,[47] which can be influenced by the types of radicals present in the reactants and the reaction conditions.[22,53,54] The enrichment factors for MDF are not listed here because we only focus on the odd-MIF in this study. [b]Odd-MIF fractionation in oxidation processes is cited from Sun et al.[24,47] [c]Enrichment factors for atmospheric $Hg^{II}(P)$ reduction to Hg^0 have not been reported directly; here we use the mean enrichment factor of photoreduction for aqueous Hg synthesized in Sun et al.[43] [d]Equations 1 and 2 are adopted from Zhu et al.,[49] in which the $\varepsilon^{202}Hg$ shows a positive correlation with Hg^0 concentration in the air (CHg^0): $\varepsilon^{202}Hg(‰) = 1.43\log_{10}(CHg^0) - 1.19$; the $E^{199}Hg$ is a negative correlation with solar radiation (SR, W m^{-2}): eq 1: $E^{199}Hg = -0.0007SR - 0.005$, eq 2: $E^{201}Hg = E^{199}Hg/1.13$, which is calculated from $\Delta^{199}Hg/\Delta^{201}Hg = 1.13$. In the model, CHg^0 is applied as the Hg^0 concentration in terms of corresponding grids, and the SR is represented by the incident shortwave radiation at the ground. [e]Photoreduction of terrestrial Hg is utilized from the synthesized from Sun et al.,[43] with the $\varepsilon^{202}Hg = -1.32‰$, $E^{199}Hg = E^{201}Hg = -1.02‰$. [f]Chamber measurement[50,55] has reported $E^{199}Hg$ of about 3.5‰ between snow and air during the Arctic AMDE. We speculate that 60% of deposited snowfall-Hg can be re-emitted to the air and estimated that the $\varepsilon^{202}Hg$ of snow-released Hg of −0.53‰, and assumed the $E^{199}Hg$ and $E^{201}Hg$ of 1.40‰ representing the level of annual re-emission. [g]Mercury isotope fractionation in the oceanic environment remains unexplored. Model studies have indicated that Hg^0 released into the ocean is subject to isotopic alteration due to reduction processes occurring within the ocean.[43,56] Drawing from investigations into Hg^{II} reduction in NOM-rich waters[51] and freshwater−air Hg^0 exchanges,[52] we hypothesize that oceanic reduction follows a similar fractionation pattern and assume the enrichment factors of $\varepsilon^{202}Hg = -0.13‰$, $E^{199}Hg = E^{201}Hg = -0.15‰$.

isotope signatures of $Hg^{II}(P)$. Our objective of this work is to evaluate atmospheric Hg chemistry mechanisms by using observed isotope signatures of $Hg^{II}(P)$ as constraints. We simulate three scenarios (Run1−3) based on recent advances in atmospheric Hg chemistry mechanisms and validate these mechanisms by comparing them with observed Hg isotope fractionations (Figure 1A). We examine the distribution of the odd-MIF of $Hg^{II}(P)$ in the atmosphere, analyze the contributing factors, and discuss the implications of our findings on current and future Hg cycling.

2. MATERIALS AND METHODS

2.1. GEOS-Chem Model. In this study, we employ the GEOS-Chem model (version 12.9.0) described by Shah et al.[8] The model utilizes assimilated meteorological data archived from the Goddard Earth Observation System (GEOS) general circulation model conducted by the NASA Global Modeling and Assimilation Office (GMAO). The model employs the native MERRA2 (4° × 5°) meteorological data. Mercury emissions from Horowitz et al.[9] are incorporated into the model, with gridded land and ocean surface Hg concentration serving as boundary conditions. The dry deposition velocity for Hg is calculated using a resistance-in-series scheme.[33] Wet scavenging of Hg^{II} [sum of $Hg^{II}(g)$ and $Hg^{II}(P)$] is included following the scheme proposed by Liu et al.[34] Mercury storage and release from snow and ice are accounted for using the snowpack-Hg-flux modules. Reactive $Hg^{II}(g)$ in the MBL is parametrized to be taken up by sea salt aerosol based on Holmes et al.[6] The transfer of $Hg^{II}(g)$ between the gas phase and the aerosol/cloud phase is treated as a temperature-dependent kinetic process, as described by Amos et al.[35] This model incorporates the latest advancements in the atmospheric Hg chemistry mechanism, which includes the oxidation of Hg^0 by both Br and OH, followed by the oxidation of Hg^I by ozone and radicals. It also involves the partitioning of Hg^{II} within aerosols and cloud droplets, as well as the photolysis of speciated Hg^{II} in both gas and aqueous phases.[8]

2.2. Atmosphere Mercury Isotope Model. The Hg isotope-related processes are simulated based on a previously developed Hg isotope model,[36] with upgrades in the chemistry mechanism and isotope fractionation. Each of the Hg isotopes (^{196}Hg, ^{198}Hg, ^{199}Hg, ^{200}Hg, ^{201}Hg, ^{202}Hg, and ^{204}Hg) is treated as an independent tracer, which results in 175 advected tracers in the model. Mercury isotopes have consistent chemical reactions but different chemistry rates. The chemical mechanisms are solved using the Kinetic Pre-Processor (KPP),[37,38] customized for GEOS-Chem, with a time step of 1 h on the model grid. The model encompasses 47 vertical layers extending to the mesosphere, with a horizontal resolution of 4° latitude × 5° longitude. We utilize the anthropogenic Hg isotope emissions in 2010 from Song et al.,[36] which include Hg isotopic signatures emitted from various sectors. These anthropogenic emissions are derived from EDGARv4.tox2, which represents the emission level from human activities at the present-day.[39] We also consider a natural source, with the integrated Hg isotopic signatures presented in Table S1. The model simulation spans from 2013 to 2016. By initializing the model with the restart file from Shah et al.,[8] we ensure that the model reaches a steady state for three years of simulation, and we analyze the results from the final year.

2.3. Isotope Notation and Fractionation. We use the same notation as in Blum and Bergquist[40] to express our simulated isotope composition. The notations are defined as the isotope ratio difference of simulated species and the NIST-3133 standard in a unit of permil (‰), with the MDF represented by $\delta^{xxx}Hg$ (‰) and the MIF represented by $\Delta^{xxx}Hg$ (‰).

https://doi.org/10.1021/acs.est.4c02600
Environ. Sci. Technol. XXXX, XXX, XXX−XXX

$$\delta^{xxx}Hg(‰) = [(^{xxx/198}Hg/^{xxx/198}Hg_{NIST3133}) - 1] \times 1000 \quad (1)$$

MIF is calculated as below:

$$\Delta^{xxx}Hg = \delta^{xxx}Hg - \delta^{202}Hg \times \beta_{xxx} \quad (2)$$

where xxx represents the mass number of Hg stable isotopes and β is taken as −0.507, 0.252, 0.502, 0.752, and 1.493 for ^{196}Hg, ^{199}Hg, ^{200}Hg, ^{201}Hg, ^{202}Hg, and ^{204}Hg, respectively. The $^{xxx}/^{198}Hg_{NIST3133}$ ratios in eq 1 are treated as constants, which are calculated from Hg atomic abundances in the NIST-3133 standard,[40,41] namely ^{196}Hg = 0.155%, ^{198}Hg = 10.04%, ^{199}Hg = 16.94%, ^{200}Hg = 23.14%, ^{201}Hg = 13.17%, ^{202}Hg = 29.73%, and ^{204}Hg = 6.83%. We synthesized the Hg isotope composition (δ and Δ) of each source and calculated its isotope ratio ($^{xxx/198}$Hg) using eqs 1 and 2. These ratios allow us to partition the total Hg emissions into seven isotopes for input into the model. Following the simulation, we can also calculate the isotope composition by using eqs 1 and 2.

In the model, Hg transfer and transformation are treated as kinetic processes. Thus, we can slightly perturb the reaction coefficients for different isotopes to achieve isotope fractionation. ^{198}Hg is taken as the reference isotope in the model, which retains the parameters (K_{198}) the same as the standard GEOS-Chem. The K_{xxx} for the other six isotopes is calculated as follows:

$$K_{xxx} = K_{198} \times \alpha^{xxx/198}Hg_{tot} \quad (3)$$

where the processes-based kinetic fractionation factors ($\alpha^{xxx/198}Hg_{tot}$) are defined as the transfer rates of the ^{xxx}Hg-to-^{198}Hg and the ratio of $^{xxx/198}$Hg for the product over reactant, including two parts: $\alpha^{xxx/198}Hg_{MDF}$ and $\alpha^{xxx/198}Hg_{MIF}$. The reported $\alpha^{xxx/198}Hg_{MDF}$ obeys the MDF kinetic laws during Hg transfer:[24,42]

$$\ln(\alpha^{xxx/198}Hg_{MDF}) = \beta_{xxx} \times \ln(\alpha^{202/198}Hg) \quad (4)$$

Previous studies have reported Hg isotope enrichment factors (ε^{xxx}Hg for MDF and E^{xxx}Hg for MIF) during many physical and chemical processes, which are calculated from the difference in the MDF and MIF signature as product over reactant Hg pools.[24,43] Processes-based kinetic fractionation factors ($\alpha^{xxx/198}$Hg) can be calculated as follows:

$$\ln(\alpha^{xxx/198}Hg_{MDF}) = \varepsilon^{xxx}Hg/1000 \quad (5)$$

$$\ln(\alpha^{xxx/198}Hg_{MIF}) = E^{xxx}Hg/1000 \quad (6)$$

The $\alpha^{xxx/198}Hg_{tot}$ is calculated as follows:

$$\alpha^{xxx/198}Hg_{tot} = \alpha^{xxx/198}Hg_{MDF} \times \alpha^{xxx/198}Hg_{MIF} \quad (7)$$

We apply the Hg isotope enrichment factors from recent remarkable studies, as presented in Table 1. Various atmospheric processes can impact the cycling of atmospheric Hg, yet the extent of Hg isotopic fractionation during these processes remains incompletely understood. While some processes, such as the sorption of dissolved Hg^{II} onto particles, abiotic dark oxidation, and the evasion of dissolved gaseous Hg^0, have been observed to cause insignificant odd-MIF effects,[44−46] our model exclusively incorporates processes known to result in significant odd-MIF. The enrichment factors measured by Sun et al.[24,47] depict the isotopic fractionation resulting from "net Hg^0" oxidation within the experimental system. These fractionations reflect the isotopic change in the reactant Hg^0. Therefore, we incorporated these enrichment factors into the initial step of Hg^0 oxidation (Table 1). This adjustment allows the model to replicate a fractionation effect similar to that observed in the experiment, wherein the reactant Hg^0 enriches odd-Hg isotopes. Subsequent oxidation of Hg^I intermediates leads to an odd-MIF signal transferring to the Hg^{II}(g) and eventually to the Hg^{II}(P).

Isotope fractionations of Hg^0 in the global atmosphere were assessed by Song et al.[36] In this study, our focus is solely on the odd-MIF of Hg^{II}(P), which serves as an indicator of the redox chemistry of atmospheric Hg. We exclude discussing the MDF as it is influenced by both physical and chemical processes.[18] While the even-MIF of Hg isotopes holds potential for reflecting redox chemistry processes,[21,24,25,48] its specific fractionation mechanism remains incompletely understood. Parameterizing the even-MIF processes in our model presents a significant challenge, and testing the even-MIF mechanism would divert from the primary focus of the current research. We intend to evaluate even-MIF fractionations using our model in future studies.

2.4. Scenario Descriptions. We consider three scenarios to investigate different chemistry mechanisms, as outlined in Table 2. Run1 and Run2 employ the same chemistry mechanism as described by Shah et al.[8] but utilize different Br fields. Run1 incorporates the Br field from Wang et al.,[17] which accounts for bromine radicals from the debromination of SSA. In Run2, tropospheric Br and BrO concentrations from Schmidt et al.[57] (0.08 and 0.48 pptv) are higher compared to Run1 (0.03 and 0.19 pptv), but lower in the MBL due to the absence of SSA debromination. Stratospheric Br concentrations in Run2 are exceeding more than twice as it in Run1, resulting in distinct vertical distribution patterns.[8] Run3 utilizes the chemistry mechanism from Horowitz et al.,[9] which also incorporates the Br field from Schmidt et al.[57] Recent advancements in atmospheric Hg chemistry, such as the oxidation of Hg^0 by OH and the photoreduction of gaseous Hg^{II}(g),[11,58] have been integrated into the chemistry mechanism proposed by Shah et al.[8] The photolysis frequencies varied between gaseous and heterogeneous Hg^{II}, with the latter including aerosols and cloudwater. The photoreduction of gaseous Hg^{II} does not lead to odd-MIF,

Table 2. Comparison of the Differences between the Three Scenarios Set in This Study

description	Run1[a]	Run2[a]	Run3[b]
Hg^0 oxidation by Br	√	√	√
Hg^0 oxidation by OH	√	√	×
Hg^0 oxidation by Cl	√	√	√
photoreduction of gaseous Hg^{II}(g)	√	√	×
Br field[c]	√	√	√
photolysis frequency of Hg^{II}(P)→Hg^0[d]	$\beta_1 \times JNO_2$	$\beta_2 \times JNO_2$	$\beta_3 \times JNO_2$

[a]Chemistry mechanism from Shah et al.[8] [b]Chemistry mechanism from Horowitz et al.[9] [c]Run1 uses Br field from Wang et al.,[59] while Run2 and Run3 from Schmidt et al.[57] [d]The photolysis frequency of Hg^{II}(P) → Hg^0 is parametrized as $\beta \times JNO_2$, where JNO_2 represents the local photolysis frequency of NO_2, and β is the scaling factor adjustable to accurately reproduce the observations of Hg^0 in the global atmosphere. The values of β_1, β_2, and β_3 are 4×10^{-3}, 4×10^{-2}, and 5.2×10^{-2}, respectively.[8,9]

https://doi.org/10.1021/acs.est.4c02600
Environ. Sci. Technol. XXXX, XXX, XXX−XXX

as water is required to hydrate the Hg-ligand radical pairs produced by photolysis.[19,53,54] The hydration creates a cage effect, extending the lifetime of the radical pair sufficiently for odd-MIF of Hg isotopes. These scenarios employ the same emission inventories[36] and fractionation factors (Table 1). The photoreduction rates for $Hg^{II}(P)$ are scaled from the local photolysis frequency of NO_2, which is tuned to match the observations of atmospheric Hg concentrations.[8]

2.5. Mercury Isotope Data. We have synthesized available observations of odd-MIF ($\Delta^{199}Hg$ and $\Delta^{201}Hg$) in land and marine aerosols, as shown in Figure 1A. These observations are based on measurements conducted on site observations or on vessels in three studies crossing from the Southern Ocean to the Arctic Ocean during the sampling period from 2015 to 2019. Most of the PBM samples were collected on quartz fiber filters, which may capture a fraction of the gaseous Hg^{II} species. On land, the data are synthesized as average values from site observations,[4,30,31,60−64] which are mainly located in Asia and North America. In MBL, Huang et al.[26] conducted three measurement cruises, collecting 52 $Hg^{II}(P)$ samples from the western North Pacific, Northwest Pacific, and the Pacific's northwest marginal region between 2018 and 2019. Qiu et al.[28] collected and analyzed Hg isotope information from 16 total suspended particle samples in the marginal seas of South and Southeast Asia in 2016. AuYang et al.[27] reported Hg isotope information from 42 marine aerosol samples collected along the cruise track from Shanghai, China, to East Antarctica from 2015 to 2016. We have synthesized the specific information, including the sampling time and locations, and utilized this data for evaluation purposes. We categorized the observations into three groups based on their respective sites: MBL and coast, terrestrial urban, and terrestrial remote (mountain sites). The median $\Delta^{199}Hg^{II}(P)$ and $\Delta^{201}Hg^{II}(P)$ for each category were as follows: 0.08‰ (interquartile range [IQR], −0.11−0.28‰; n = 112) and 0.05‰ (IQR, −0.09−0.22‰; n = 113) for MBL and coast, 0.10‰ (IQR, −0.03−0.33‰; n = 14) and 0.03‰ (IQR, −0.06−0.20‰; n = 14) for terrestrial urban, and 0.40‰ (IQR, 0.34−0.49‰; n = 4) and 0.35‰ (IQR, 0.25−0.47‰; n = 4) for terrestrial remote, respectively. Collectively, the global observed $\Delta^{199}Hg^{II}(P)$ and $\Delta^{201}Hg^{II}(P)$ values ranged from −0.90‰ to 0.71‰ (with an average of 0.08 ± 0.29‰, n = 131) and −0.74‰ to 0.73‰ (with an average of 0.06 ± 0.27‰, n = 130), respectively. We excluded polar observations from our study due to the incomplete knowledge of atmospheric Hg isotope fractionation in polar regions.

2.6. Uncertainty. The uncertainties in our model primarily stem from the Hg isotope fractionation of source emissions and atmospheric redox chemistry processes. The odd-MIF composition of oceanic sources, cited from Jiskra et al.,[65] has an uncertainty of about ±0.10‰. The enrichment factors ($E^{199}Hg$ and $E^{201}Hg$) for odd-MIF in Hg^0 oxidation processes (e.g., oxidation by Br, OH, and Cl) also fluctuate within ±0.10‰, while the enrichment factors for odd-MIF in photoreduction are based on Zheng and Hintelmann,[23] with an uncertainty of ±0.14‰. Given that these uncertainties collectively impact the simulated odd-MIF values of $Hg^{II}(P)$, we combine the enrichment factors of each process, considering their respective fluctuation ranges, to evaluate the model's uncertainty. For instance, we opt for the upper limits of the oceanic source (+0.10‰) and Hg^0 oxidation (+0.10‰), while adopting the lower limit for photoreduction of $Hg^{II}(P)$ (−0.14‰) to simulate the upper end of $\Delta^{199}Hg^{II}(P)$ and $\Delta^{201}Hg^{II}(P)$, and vice versa for the lower end. The simulated ranges of $\Delta^{199}Hg^{II}(P)$ and $\Delta^{201}Hg^{II}(P)$ at the observed sites are 0.00−0.08‰ and 0.02−0.09‰, respectively, which are still within the error range of the observations (0.04 ± 0.29‰ and 0.06 ± 0.29‰, respectively). This suggests that uncertainties in oceanic emissions and redox enrichment factors do not cause significant fluctuations in the model's results for $\Delta^{199}Hg^{II}(P)$ and $\Delta^{201}Hg^{II}(P)$.

Another source of uncertainty arises from the knowledge gaps surrounding Hg isotope fractionations within biogeochemical processes. We assume the isotopic enrichment factors ($E^{199}Hg$ and $E^{201}Hg$) in the photoreduction of Hg^{II} in snowpack and the ocean following previous studies (Table 1), which is similar to that of photoreduction of $Hg^{II}(P)$ in the atmosphere, a representative for natural systems. In addition, previous studies found that the direction of MIF of the Hg isotope in polar regions appears to differ from that in other regions,[60,62,66] possibly due to the presence of oxidants and binding ligands in the air.[66] Our simulation results for the polar oceans may include potential biases, as our model assumes a global uniform odd-Hg isotope fractionation. Furthermore, Huang et al.[30] found that the magnitude and sign of MIF depend on soot aerosol water content, which may have impact on our simulation results on land as we could not parametrize this process at the current stage. Moreover, the enrichment factors may vary with temperature and pressure in the atmosphere,[25] which could affect our simulation results since we employed enrichment factors reported under specific temperature (298 K) and pressure (750 Torr) conditions.[24] Given the scarcity of studies reporting enrichment factors of atmospheric Hg under various environmental conditions, our parametrization in the model represents the best available approach. Further laboratory or field studies focusing on Hg isotope fractionation in these key processes are necessary to obtain more accurate enrichment factors.

Uncertainty may also arise when comparing the simulated and observed data. The observations synthesized in this study span the past decade, while our model results pertain to the year 2016. Consequently, the potential for interannual discrepancies between simulations and observations cannot be discounted. Observations are sampled over limited time frames, particularly in the MBL, and our model employs annual averages. Therefore, there remains the possibility that observations may not fully capture the annual average results of the model during certain brief periods. Additionally, our model's results exclusively analyze the isotopic composition of the PBM. In contrast, actual observations may exhibit mixed isotopic signals due to differences in sampling techniques. For instance, observations at the Pic du Midi Observatory encompass an isotopic blend of gaseous Hg^{II} and PBM.[20]

3. RESULTS AND DISCUSSION

3.1. Odd-MIF Signatures in the Scenarios. The three scenarios (Run1−3) simulate drastically different odd-MIF of $Hg^{II}(P)$ [$\Delta^{199}Hg^{II}(P)$ and $\Delta^{201}Hg^{II}(P)$] in the global atmosphere (Figure S1), even though all reproduce the global spatial variability of observed TGM and wet deposition (see Supporting Information Appendix, Text S1). We synthesized globe observations of $\Delta^{199}Hg^{II}(P)$ and $\Delta^{201}Hg^{II}(P)$ that contain sites in land and MBL (Figure 1A).[4,20,26−29,31,60−64,67−75] We find that Run1 simulates $\Delta^{199}Hg^{II}(P)$ and $\Delta^{201}Hg^{II}(P)$ values (0.04 ± 0.29‰ and 0.05 ± 0.29‰, respectively) comparable to observations (0.08

https://doi.org/10.1021/acs.est.4c02600
Environ. Sci. Technol. XXXX, XXX, XXX−XXX

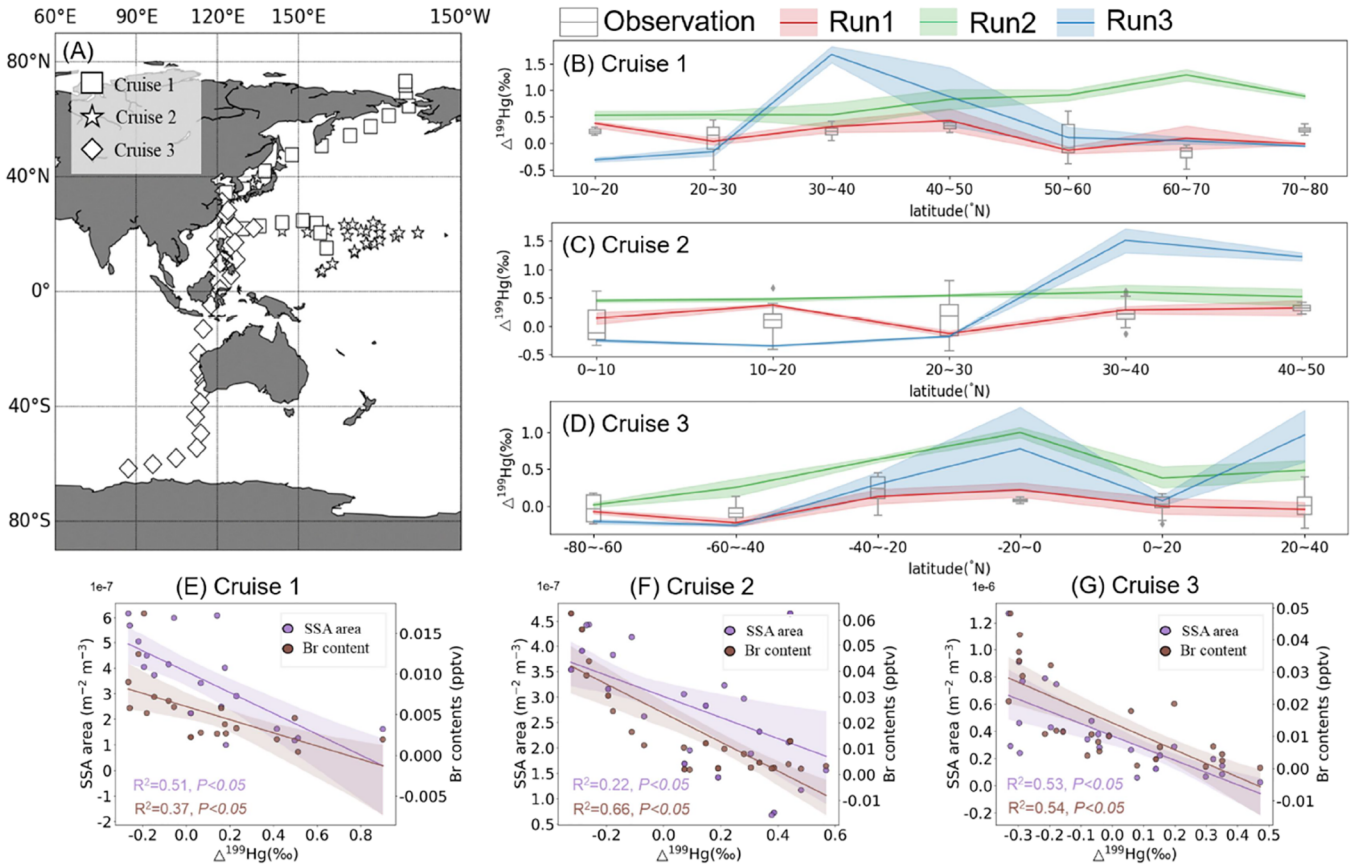

Figure 2. (A) Plot of the three selected cruises. Points in the cruises are sampled from Huang et al.,[26] Qiu et al.,[28] and AuYang et al.,[27] which are divided into cruises 1, 2, and 3. (B–D) Latitude variations of $\Delta^{199}Hg^{II}(P)$ in three selected cruises' observations and simulations. In panels B–D, the box plots represent observations. The red, green, and blue lines represent simulated $\Delta^{199}Hg^{II}(P)$ through Run1, Run2, and Run3 scenarios, respectively. (E–G) Plots of $\Delta^{199}Hg^{II}(P)$ vs. SSA areas and Br contents in Run1 of the three cruises. The SSA area data is from the updated aerosol fields of the standard GEOS-Chem simulation (version 12.9).[8]

± 0.29‰ and 0.06 ± 0.27‰, respectively). Moreover, only Run1 produces comparable $\Delta^{199}Hg^{II}(P)$ and $\Delta^{201}Hg^{II}(P)$ values across the three categorized observations (Table S2). Specifically, the median $\Delta^{199}Hg^{II}(P)$ and $\Delta^{201}Hg^{II}(P)$ in Run1 are −0.06‰ (IQR, −0.24–0.16‰) and −0.02‰ (IQR, −0.24–0.18‰) for MBL & coast regions, 0.20‰ (IQR, 0.10–0.30‰) and 0.20‰ (IQR, 0.10–0.31‰) for terrestrial urban areas, and 0.30‰ (IQR, 0.10–0.60‰) and 0.30‰ (IQR, 0.11–0.61‰) for terrestrial remote regions. In contrast, the other two scenarios yield substantially higher $\Delta^{199}Hg^{II}(P)$ and $\Delta^{201}Hg^{II}(P)$ values, with means of 0.57 ± 0.37 and 0.57 ± 0.36‰ for Run2, and 0.44 ± 0.74 and 0.47 ± 0.73‰ for Run3, respectively. The overestimation is even more distinct in the MBL and coast areas for Run2, as well as in urban and remote areas for Run3 (Figure S1, Table S2). These disparities among the scenarios arise from the variability in chemical pathways and rates, including different Br concentration fields and photolysis rates of $Hg^{II}(P)$ to Hg^0 (refer to Table 2 in Methods), which results in different redox rates in the atmosphere and causes the differences in $\Delta^{199}Hg^{II}(P)$ and $\Delta^{201}Hg^{II}(P)$ values.

3.2. Impact of SSA Debromination. The different odd-MIF signatures among scenarios highlight the significant impact of SSA debromination on the atmospheric Hg chemistry in the MBL. We analyze odd-MIF data collected during three cruises covering the Southern Ocean to the Arctic Oceans (Figure 2A). Given that $\Delta^{199}Hg^{II}(P)$ and $\Delta^{201}Hg^{II}(P)$ are affected by similar factors and exhibit parallel variations, we focus on $\Delta^{199}Hg^{II}(P)$ as a representative. Figure 2B–D shows that only Run1 can reproduce the observed latitudinal $\Delta^{199}Hg^{II}(P)$ in all three cruises, whereas both Run2 and Run3 show biased values. Our analysis, based on Run1 simulation, reveals significant negative correlations of $\Delta^{199}Hg^{II}(P)$ with Br contents and SSA areas (Figure 2E–G). The Br radicals in MBL are mainly from SSA debromination processes relative to seawater composition, which has been evaluated by previous studies.[59,76,77] The noticeable correlations suggest that the SSA debromination process can significantly influence the redox rates of atmospheric Hg. Run2 and Run3, on the other hand, utilize Br concentration fields from another study,[57] which fails to account for SSA debromination. This results in much lower Br contents in the MBL,[8] and causes biased $\Delta^{199}Hg^{II}(P)$ values and $Hg^{II}(P)$ concentrations (see Supporting Information Appendix, Text S1) due to much lower oxidation rates. These findings underscore the substantial impact of SSA debromination on atmospheric Hg chemistry in the MBL and suggest that Hg isotopes can provide constraints on the redox rates. It also has a significant impact on the global atmosphere, as the MBL hosts active redox reactions and air-sea exchange for Hg.[78,79] In addition, Hg^0 oxidation in the MBL accounts for over 90% of the total oxidation in the global plant boundary layer based on Run1.

https://doi.org/10.1021/acs.est.4c02600
Environ. Sci. Technol. XXXX, XXX, XXX−XXX

3.3. Constraining $Hg^{II}(P)$ Photoreduction Rates. Our simulations provide insights into the photoreduction rate of $Hg^{II}(P)$ in the atmosphere, which shows a significant fluctuation across various mechanisms responding to different oxidation rates influenced by the Br concentration fields. We find that the discrepancy of Run2 and Run3 with observed $\Delta^{199}Hg^{II}(P)$ can be mainly attributable to an overestimation of the rates of $Hg^{II}(P)$ photoreduction. The reduction rates in the three scenarios follow the order of Run3 (5.2×10^{-2} JNO_2) > Run2 (4.0×10^{-2} JNO_2) > Run1 (4.0×10^{-3} JNO_2) (where preceding numbers are scaling factors, as detailed in Table 2). Notably, Run1 and Run2 share the same chemistry mechanism.[8] However, the simulated $\Delta^{199}Hg^{II}(P)$ values in Run2 are notably overestimated in comparison to observations and Run1 when the scale factors increase from the magnitude of 10^{-3} to 10^{-2} (Figure S2). Run3, utilizing a distinct chemistry mechanism,[9] similarly exhibits significantly overestimated $\Delta^{199}Hg^{II}(P)$ values when employing a scale factor at the magnitude of 10^{-2}, particularly in terrestrial and near-shore regions (Figure S2). It is known that Hg^0 oxidation and $Hg^{II}(P)$ photoreduction processes compete to shape the odd-MIF of $Hg^{II}(P)$, with the former leading to negative and the latter to positive $\Delta^{199}Hg^{II}(P)$ and $\Delta^{201}Hg^{II}(P)$ values (Figure 1B–G and Table 1 in Methods).[20,25,43,51] Although the oxidation rates are higher than those of photoreduction in the atmosphere,[8,9] i.e., a net oxidation from Hg^0 to Hg^{II}, our study demonstrates that the photoreduction process plays a more important role in deciding the odd-MIF of $Hg^{II}(P)$ across most of the atmosphere (Figure S1). This is associated with a higher isotopic enrichment factor for the photoreduction process than the oxidation (see Supporting Information Appendix, Text S2).

3.4. Constraining Atmospheric Hg Chemistry. These findings demonstrate that isotopes can provide additional insights into atmospheric Hg chemistry beyond the total Hg observations. By simulating with different chemistry mechanisms, we find that a wide combination of gross oxidation and reduction rates can reproduce the observed total Hg concentrations and deposition fluxes (gray shade area in Figure 3). Indeed, the observed TGM concentrations and wet deposition data primarily serve as constraints on net redox rates (i.e., the difference between the gross oxidation and reduction rates), as these observations can be effectively reproduced by adjusting the relative magnitude of these chemical reaction rates. However, the Hg isotope signatures demonstrate the significant role of the SSA debromination. Considering all the odd-MIF observational data worldwide (Figure 1A), our scenarios collectively indicate that the rate of $Hg^{II}(P)$ photoreduction in the global atmosphere should be at the magnitude of 10^{-3} JNO_2. This implies an annual photoreduction of $Hg^{II}(P)$ of approximately 4 Gg yr^{-1} in the global atmosphere, which is much lower than the rates depicted in Run2 and Run3 (approximately 10 Gg yr^{-1}) and many previous studies.[6,8,9] These findings are also corroborated by experimental research that has suggested a low rate of aqueous-phase photoreduction.[9,11,80] Overall, the isotope constraints result in a collapse of the uncertainty range in Hg redox chemistry in the atmosphere (Figure 3). Based on these results, we suggest that the chemical mechanism employed in Run1 might be more applicable, as it effectively reproduces both the global atmospheric Hg concentrations (including Hg wet deposition) and the odd-MIF of $Hg^{II}(P)$ in the atmosphere.

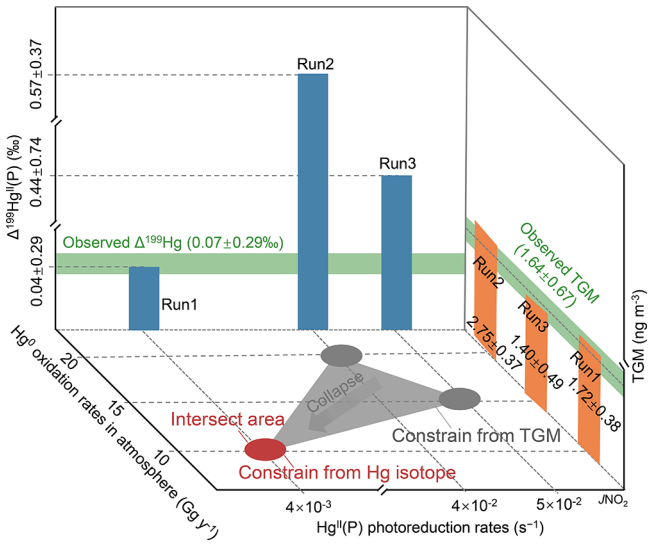

Figure 3. Isotope data constrain the redox chemistry rates of Hg in the atmosphere. The gray shade area represents the redox chemistry rates constrained by observed TGM concentrations, and the red intersect area represents the redox chemistry rates constrained by both observed TGM and Hg isotope data. The green shade area represents the mean (±SD) of observed Hg isotope data in MBL and global observed TGM.

The simulation results can also contribute to resolving the uncertainty surrounding the Hg^0 oxidation pathway in MBL, specifically whether it occurs through oxidation by OH or Br.[6,7,12,81] A model study[8] that incorporates both of these oxidants suggests comparable contributions to the global net oxidation of Hg^0 to Hg^{II}. However, recent isotope data have raised uncertainties regarding the Hg^0 oxidation pathway in the MBL. For instance, based on cross-hemispheric sulfur and Hg isotope data on marine aerosols, AuYang et al.[27] proposed that Hg oxidation is primarily driven by OH/O_3 in the tropics, transitioning to Br/Cl in polar regions. On the other hand, Yu et al.[29] and Qiu et al.[28] found that Hg^0 oxidation in North Hemisphere tropical and temperate MBL is mainly initiated by Br through Hg isotope analysis. In our isotope modeling (Run1), we consider both Br and OH as important oxidants for Hg^0 and successfully reproduce the cross-hemispheric measurements of $\Delta^{199}Hg^{II}(P)$ [and $\Delta^{201}Hg^{II}(P)$]. The chemistry mechanism in our model suggests a much higher rate of Hg^0 oxidation by Br than OH in the global MBL (Figure S3). Although OH radicals have a significant effect on the global oxidation of Hg^0, most OH oxidations occur in the high-altitude troposphere (Figure S4).[8] Considering the SSA debromination, we therefore propose that Br-initiated oxidation is likely the dominant pathway for Hg^0 oxidation in the global MBL.

4. IMPLICATIONS

This study demonstrates the utility of Hg isotope modeling in linking molecular-level isotopic fractionation to global Hg cycles. Our research has significant implications for global Hg cycling. First, the constrained rate of $Hg^{II}(P)$ photoreduction in the global atmosphere marks a departure from treating this rate as a purely tuning parameter. Second, the odd-MIF data demonstrate the elevated Br radical contents in the MBL, which help illustrate the spatial pattern of Hg redox processes and transport within the atmosphere. Specifically, the con-

https://doi.org/10.1021/acs.est.4c02600
Environ. Sci. Technol. XXXX, XXX, XXX−XXX

strained Hg chemistry suggests intense Hg^0 oxidation in the MBL, resulting in a higher Hg^{II} deposition (including dry and wet deposition) into the ocean (3.2 Gg y^{-1} by Run1 vs 2.0 Gg y^{-1} by Run2), which is the substrate for the more toxic methylmercury species that pose direct risks to humans through seafood consumption. Third, the constrained chemistry indicates a higher Hg^{II} deposition onto land (1.9 Gg y^{-1} by Run1 vs 1.1 Gg y^{-1} by Run2), resulting in a 0.2 Gg increase in the annual re-emission of Hg from land. The deposition of Hg^0 to the land also shows a decrease from 2.6 Gg y^{-1} to 1.6 Gg y^{-1}. Overall, the odd-MIF signatures suggest a shorter chemical lifetime of Hg^0 against oxidation to Hg^{II} in the global atmosphere (4.5 months in Run1 vs 6.6 months in Run2), which indicates more intense of Hg^{II} deposition, suggesting a smaller sensitivity of land and ocean Hg concentrations to anthropogenic emission reductions. This aligns well with a previous study that incorporated even-MIF signatures of the ocean,[65] both suggesting more aggressive emission controls to ensure the effectiveness of the Minamata Convention on Mercury.

We find distinct patterns in the distribution of the odd-MIF of $Hg^{II}(P)$ across the atmosphere resulting from its redox chemistry. This exerts a substantial impact on the isotopic composition of Hg in terrestrial and marine environments, given that atmospheric deposition serves as a major source for both. Consequently, the mixture model studies that need accurate Hg isotope signatures of the atmosphere to track sources and transformations of Hg in the environment should account for these spatial variations. In addition, SSA debromination is influenced by various environmental variables such as wind patterns, sea-surface temperatures, and aerosol acidity.[16,59] As environmental shifts persist, including ocean warming,[82] acidification,[83,84] and eutrophication,[85,86] we anticipate consequential effects on the SSA concentrations and Br debromination processes. These alterations, in turn, will ripple through atmospheric Hg redox chemistry and broader global Hg cycles.

■ ASSOCIATED CONTENT

Supporting Information

The Supporting Information is available free of charge at https://pubs.acs.org/doi/10.1021/acs.est.4c02600.

Additional information about model evaluation and quantifying the redox effects on odd-MIF; spatial pattern of shifting of odd-MIF caused by redox chemistry, simulated odd-MIF, and redox chemistry rates; vertical distribution of Hg^0 gross oxidation rates; isotope signatures of Hg end-members; observed and simulated odd-MIF values; and observed and simulated TGM concentrations, wet deposition flux, and PBM concentrations (PDF)

Observed Hg isotope data (XLSX)

■ AUTHOR INFORMATION

Corresponding Author

Yanxu Zhang − *School of Atmospheric Sciences and Frontiers Science Center for Critical Earth Material Cycling, Nanjing University, Nanjing, Jiangsu 210023, China;* orcid.org/0000-0001-7770-3466; Email: zhangyx@nju.edu.cn

Authors

Zhengcheng Song − *School of Atmospheric Sciences and Frontiers Science Center for Critical Earth Material Cycling, Nanjing University, Nanjing, Jiangsu 210023, China;* orcid.org/0009-0001-4298-8243

Shaojian Huang − *School of Atmospheric Sciences, Nanjing University, Nanjing, Jiangsu 210023, China*

Peng Zhang − *School of Atmospheric Sciences, Nanjing University, Nanjing, Jiangsu 210023, China*

Tengfei Yuan − *School of Atmospheric Sciences, Nanjing University, Nanjing, Jiangsu 210023, China*

Complete contact information is available at: https://pubs.acs.org/10.1021/acs.est.4c02600

Notes

The authors declare no competing financial interest.

■ ACKNOWLEDGMENTS

This work was funded by the National Natural Science Foundation of China (grant No. 42307331, 42394094, 42177349, and 41776048), the Fundamental Research Funds for the Central Universities, China (0207-14380188 and 0207-14380168), the "GeoX" Interdisciplinary Research Funds for Frontiers Science Center for Critical Earth Material Cycling, Nanjing University, and the Collaborative Innovation Center of Climate Change, Jiangsu Province.

■ REFERENCES

(1) Zhang, Y.; Song, Z.; Huang, S.; Zhang, P.; Peng, Y.; Wu, P.; Gu, J.; Dutkiewicz, S.; Zhang, H.; Wu, S.; Wang, F.; Chen, L.; Wang, S.; Li, P. Global health effects of future atmospheric mercury emissions. *Nat. Commun.* **2021**, *12*, 3035.

(2) Feng, L.; Zhang, C. C.; Liu, H. H.; Li, P.; Hu, X. F.; Wang, H. Q.; Chan, H. M.; Feng, X. N. Impact of low-level mercury exposure on intelligence quotient in children via rice consumption. *Ecotox Environ. Safe* **2020**, *202*, ARTN 110870.

(3) Chen, L.; Liang, S.; Liu, M. D.; Yi, Y. J.; Mi, Z. F.; Zhang, Y. X.; Li, Y. M.; Qi, J. C.; Meng, J.; Tang, X.; Zhang, H. R.; Tong, Y. D.; Zhang, W.; Wang, X. J.; Shu, J.; Yang, Z. F. Trans-provincial health impacts of atmospheric mercury emissions in China. *Nat. Commun.* **2019**, *10*, ARTN 1484.

(4) Liu, C.; Fu, X.; Xu, Y.; Zhang, H.; Wu, X.; Sommar, J.; Zhang, L.; Wang, X.; Feng, X. Sources and Transformation Mechanisms of Atmospheric Particulate Bound Mercury Revealed by Mercury Stable Isotopes. *Environ. Sci. Technol.* **2022**, *56*, 5224−5233.

(5) Beckers, F.; Rinklebe, J. Cycling of mercury in the environment: Sources, fate, and human health implications: A review. *Critical Reviews in Environmental Science and Technology* **2017**, *47*, 693−794.

(6) Holmes, C. D.; Jacob, D. J.; Corbitt, E. S.; Mao, J.; Yang, X.; Talbot, R.; Slemr, F. Global atmospheric model for mercury including oxidation by bromine atoms. *Atmospheric Chemistry and Physics* **2010**, *10*, 12037−12057.

(7) Selin, N. E.; Jacob, D. J.; Yantosca, R. M.; Strode, S.; Jaegle, L.; Sunderland, E. M. Global 3-D land-ocean-atmosphere model for mercury: Present-day versus preindustrial cycles and anthropogenic enrichment factors for deposition (vol 22, artn no GB3099, 2008). *Global Biogeochemical Cycles* **2008**, *22*, Artn Gb3099.

(8) Shah, V.; Jacob, D. J.; Thackray, C. P.; Wang, X.; Sunderland, E. M.; Dibble, T. S.; Saiz-Lopez, A.; Černušák, I.; Kellö, V.; Castro, P. J.; Wu, R.; Wang, C. Improved Mechanistic Model of the Atmospheric Redox Chemistry of Mercury. *Environ. Sci. Technol.* **2021**, *55*, 14445.

(9) Horowitz, H. M.; Jacob, D. J.; Zhang, Y.; Dibble, T. S.; Slemr, F.; Amos, H. M.; Schmidt, J. A.; Corbitt, E. S.; Marais, E. A.; Sunderland, E. M. A new mechanism for atmospheric mercury redox chemistry: implications for the global mercury budget. *Atmospheric Chemistry and Physics* **2017**, *17*, 6353−6371.

(10) Pacyna, J. M.; Travnikov, O.; De Simone, F.; Hedgecock, I. M.; Sundseth, K.; Pacyna, E. G.; Steenhuisen, F.; Pirrone, N.; Munthe, J.; Kindbom, K. Current and future levels of mercury atmospheric pollution on a global scale. *Atmospheric Chemistry and Physics* **2016**, *16*, 12495−12511.
(11) Saiz-Lopez, A.; Sitkiewicz, S. P.; Roca-Sanjuan, D.; Oliva-Enrich, J. M.; Davalos, J. Z.; Notario, R.; Jiskra, M.; Xu, Y.; Wang, F.; Thackray, C. P.; Sunderland, E. M.; Jacob, D. J.; Travnikov, O.; Cuevas, C. A.; Acuna, A. U.; Rivero, D.; Plane, J. M. C.; Kinnison, D. E.; Sonke, J. E. Photoreduction of gaseous oxidized mercury changes global atmospheric mercury speciation, transport and deposition. *Nat. Commun.* **2018**, *9*, 4796.
(12) Ariya, P.; Peterson, K.; Snider, G.; Amyot, M. *Mercury Chemical Transformations in the Gas, Aqueous and Heterogeneous Phases: State-of-the-Art Science and Uncertainties*; Springer: 2009.
(13) Saiz-Lopez, A.; Travnikov, O.; Sonke, J. E.; Thackray, C. P.; Jacob, D. J.; Carmona-Garcia, J.; Frances-Monerris, A.; Roca-Sanjuan, D.; Acuna, A. U.; Davalos, J. Z.; Cuevas, C. A.; Jiskra, M.; Wang, F.; Bieser, J.; Plane, J. M. C.; Francisco, J. S. Photochemistry of oxidized Hg(I) and Hg(II) species suggests missing mercury oxidation in the troposphere. *Proc. Natl. Acad. Sci. U.S.A.* **2020**, *117*, 30949−30956.
(14) Saiz-Lopez, A.; Acuna, A. U.; Trabelsi, T.; Carmona-Garcia, J.; Davalos, J. Z.; Rivero, D.; Cuevas, C. A.; Kinnison, D. E.; Sitkiewicz, S. P.; Roca-Sanjuan, D.; Francisco, J. S. Gas-Phase Photolysis of Hg(I) Radical Species: A New Atmospheric Mercury Reduction Process. *J. Am. Chem. Soc.* **2019**, *141*, 8698−8702.
(15) Donohoue, D. L.; Bauer, D.; Cossairt, B.; Hynes, A. J. Temperature and Pressure Dependent Rate Coefficients for the Reaction of Hg with Br andthe Reaction of Br with Br: A Pulsed Laser Photolysis-Pulsed Laser Induced Fluorescence Study. *J. Phys. Chem. A* **2006**, *110*, 6579−7009.
(16) Jiang, B.; Xie, Z.; Lam, P. K. S.; He, P.; Yue, F.; Wang, L.; Huang, Y.; Kang, H.; Yu, X.; Wu, X. Spatial and Temporal Distribution of Sea Salt Aerosol Mass Concentrations in the Marine Boundary Layer From the Arctic to the Antarctic. *J. Geophys. Res.: Atmos.* **2021**, *126*, No. e2020JD033892, DOI: 10.1029/2020JD033892.
(17) Wang, X.; Jacob, D. J.; Eastham, S. D.; Sulprizio, M. P.; Zhu, L.; Chen, Q.; Alexander, B.; Sherwen, T.; Evans, M. J.; Lee, B. H.; Haskins, J. D.; Lopez-Hilfiker, F. D.; Thornton, J. A.; Huey, G. L.; Liao, H. The role of chlorine in global tropospheric chemistry. *Atmospheric Chemistry and Physics* **2019**, *19*, 3981−4003.
(18) Blum, J. D.; Sherman, L. S.; Johnson, M. W. Mercury Isotopes in Earth and Environmental Sciences. *Annual Review of Earth and Planetary Sciences* **2014**, *42*, 249−269.
(19) Bergquist, B. A.; Blum, J. D. Mass-Dependent and -Independent Fractionation of Hg Isotopes by Photoreduction in Aquatic Systems. *Science* **2007**, *318*, 417−420.
(20) Fu, X.; Jiskra, M.; Yang, X.; Marusczak, N.; Enrico, M.; Chmeleff, J.; Heimburger-Boavida, L. E.; Gheusi, F.; Sonke, J. E. Mass-Independent Fractionation of Even and Odd Mercury Isotopes during Atmospheric Mercury Redox Reactions. *Environ. Sci. Technol.* **2021**, *55*, 10164−10174.
(21) Chen, J. B.; Hintelmann, H.; Feng, X. B.; Dimock, B. Unusual fractionation of both odd and even mercury isotopes in precipitation from Peterborough, ON, Canada. *Geochim. Cosmochim. Acta* **2012**, *90*, 33−46.
(22) Zheng, W.; Hintelmann, H. Isotope Fractionation of Mercury during Its Photochemical Reduction by Low-Molecular-Weight Organic Compounds. *J. Phys. Chem. A* **2010**, *114*, 4246−4253.
(23) Zheng, W.; Hintelmann, H. Mercury isotope fractionation during photoreduction in natural water is controlled by its Hg/DOC ratio. *Geochim. Cosmochim. Acta* **2009**, *73*, 6704−6715.
(24) Sun, G.; Sommar, J.; Feng, X.; Lin, C. J.; Ge, M.; Wang, W.; Yin, R.; Fu, X.; Shang, L. Mass-Dependent and -Independent Fractionation of Mercury Isotope during Gas-Phase Oxidation of Elemental Mercury Vapor by Atomic Cl and Br. *Environ. Sci. Technol.* **2016**, *50*, 9232−9241.
(25) Sun, G.; Feng, X.; Yin, R.; Wang, F.; Lin, C. J.; Li, K.; Sommar, J. O. Dissociation of Mercuric Oxides Drives Anomalous Isotope Fractionation during Net Photo-oxidation of Mercury Vapor in Air. *Environ. Sci. Technol.* **2022**, *56*, 13428−13438.
(26) Huang, S.; Huo, Y.; Sun, H.; Lv, S.; Zhao, Y.; Lin, K.; Chen, Y.; Zhang, Y. Evidence for mass independent fractionation of even mercury isotopes in the troposphere. *Atmos. Chem. Phys. Discuss.* **2022**, *2022*, 1−42.
(27) AuYang, D.; Chen, J.; Zheng, W.; Zhang, Y.; Shi, G.; Sonke, J. E.; Cartigny, P.; Cai, H.; Yuan, W.; Liu, L.; Gai, P.; Liu, C. *South-Hemispheric Marine Aerosol Hg and S Isotope Compositions Reveal Different Oxidation Pathways*; National Science Open, 2022. DOI: 10.1051/nso/2021001.
(28) Qiu, Y.; Gai, P.; Yue, F.; Zhang, Y.; He, P.; Kang, H.; Yu, X.; Lam, P. K. S.; Chen, J.; Xie, Z. Stable mercury isotopes revealing photochemical processes in the marine boundary layer. *J. Geophys. Res.: Atmos.* **2021**, *126*, No. e2021JD034630, DOI: 10.1029/2021JD034630.
(29) Yu, B.; Yang, L.; Wang, L. L.; Liu, H. W.; Xiao, C. L.; Liang, Y.; Liu, Q.; Yin, Y. G.; Hu, L. G.; Shi, J. B.; Jiang, G. B. New evidence for atmospheric mercury transformations in the marine boundary layer from stable mercury isotopes. *Atmospheric Chemistry and Physics* **2020**, *20*, 9713−9723.
(30) Huang, Q.; He, X.; Huang, W.; Reinfelder, J. R. Mass-Independent Fractionation of Mercury Isotopes during Photo-reduction of Soot Particle Bound Hg(II). *Environ. Sci. Technol.* **2021**, *55*, 13783−13791.
(31) Fu, X.; Zhang, H.; Liu, C.; Zhang, H.; Lin, C. J.; Feng, X. Significant Seasonal Variations in Isotopic Composition of Atmospheric Total Gaseous Mercury at Forest Sites in China Caused by Vegetation and Mercury Sources. *Environ. Sci. Technol.* **2019**, *53*, 13748−13756.
(32) Zheng, W.; Gilleaudeaua, G. J.; Kah, L. C.; Anbar, A. D. Mercury isotope signatures record photic zone euxinia in the Mesoproterozoic ocean. *Proc. Natl. Acad. Sci. U. S. A.* **2018**, *115*, 10594−10599.
(33) Wesely, M. L. Parameterization of Surface Resistances to Gaseous Dry Deposition in Regional-Scale Numerical-Models. *Atmos. Environ.* **1989**, *23*, 1293−1304.
(34) Liu, H. Y.; Jacob, D. J.; Bey, I.; Yantosca, R. M. Constraints from Pb-210 and Be-7 on wet deposition and transport in a global three-dimensional chemical tracer model driven by assimilated meteorological fields. *J. Geophys Res-Atmos* **2001**, *106*, 12109−12128.
(35) Amos, H. M.; Jacob, D. J.; Holmes, C. D.; Fisher, J. A.; Wang, Q.; Yantosca, R. M.; Corbitt, E. S.; Galarneau, E.; Rutter, A. P.; Gustin, M. S.; Steffen, A.; Schauer, J. J.; Graydon, J. A.; Louis, V. L. S.; Talbot, R. W.; Edgerton, E. S.; Zhang, Y.; Sunderland, E. M. Gas-particle partitioning of atmospheric Hg(II) and its effect on global mercury deposition. *Atmospheric Chemistry and Physics* **2012**, *12*, 591−603.
(36) Song, Z.; Sun, R.; Zhang, Y. Modeling mercury isotopic fractionation in the atmosphere. *Environmental pollution* **2022**, *307*, No. 119588.
(37) Santillana, M.; Le Sager, P.; Jacob, D. J.; Brenner, M. P. An adaptive reduction algorithm for efficient chemical calculations in global atmospheric chemistry models. *Atmos. Environ.* **2010**, *44*, 4426−4431.
(38) 1680−7324/acp/2006−6-187 Sandu, A.; Sander, R. Technical note: Simulating chemical systems in Fortran90 and Matlab with the Kinetic PreProcessor KPP-2.1; Atmos. *Chem. Phys.* **2006**, *6*, 187−195.
(39) Muntean, M.; Janssens-Maenhout, G.; Song, S.; Giang, A.; Selin, N. E.; Zhong, H.; Zhao, Y.; Olivier, J. G. J.; Guizzardi, D.; Crippa, M.; Schaaf, E.; Dentener, F. Evaluating EDGARv4.tox2 speciated mercury emissions ex-post scenarios and their impacts on modelled global and regional wet deposition patterns. *Atmos. Environ.* **2018**, *184*, 56−68.
(40) Blum, J. D.; Bergquist, B. A. Reporting of variations in the natural isotopic composition of mercury. *Anal. Bioanal. Chem.* **2007**, *388*, 353−359.

https://doi.org/10.1021/acs.est.4c02600
Environ. Sci. Technol. XXXX, XXX, XXX−XXX

(41) Blum, J. D., *Applications of Stable Mercury Isotopes to Biogeochemistry*. In Handbook of Environmental Isotope Geochemistry, 2012; pp 229−245.
(42) Yang, S.; Liu, Y. Nuclear volume effects in equilibrium stable isotope fractionations of mercury, thallium and lead. *Sci. Rep.* **2015**, *5*, 12626.
(43) Sun, R.; Jiskra, M.; Amos, H. M.; Zhang, Y.; Sunderland, E. M.; Sonke, J. E. Modelling the mercury stable isotope distribution of Earth surface reservoirs: Implications for global Hg cycling. *Geochim. Cosmochim. Acta* **2019**, *246*, 156−173.
(44) Wiederhold, J. G.; Christopher, J. C.; Daniel, K.; Infante, I.; Bourdon, B.; Kretzschmar, R. Equilibrium Mercury Isotope Fractionation between Dissolved Hg(II) Species and Thiol-Bound Hg. *Environ. Sci. Technol.* **2010**, *44*, 4191−4197.
(45) Zheng, W.; Foucher, D.; Hintelmann, H. Mercury isotope fractionation during volatilization of Hg(0) from solution into the gas phase. *J. Anal Atom Spectrom* **2007**, *22*, 1097−1104.
(46) Zheng, W.; Demers, J. D.; Lu, X.; Bergquist, B. A.; Anbar, A. D.; Blum, J. D.; Gu, B. Mercury Stable Isotope Fractionation during Abiotic Dark Oxidation in the Presence of Thiols and Natural Organic Matter. *Environ. Sci. Technol.* **2019**, *53*, 1853−1862.
(47) Sun, G. Y., Mercury Isotope Fractionation during Important Chemical Conversion Processes in Atmosphere; Institute of Geochemistry, 2018, Ph.D Thesis http://dpaper.las.ac.cn/Dpaper/paperbuy.
(48) Cai, H. M.; Chen, J. B. Mass-independent fractionation of even mercury isotopes. *Sci. Bull.* **2016**, *61*, 116−124.
(49) Zhu, W.; Fu, X.; Zhang, H.; Liu, C.; Skyllberg, U.; Sommar, J.; Yu, B.; Feng, X. Mercury Isotope Fractionation during the Exchange of Hg(0) between the Atmosphere and Land Surfaces: Implications for Hg(0) Exchange Processes and Controls. *Environ. Sci. Technol.* **2022**, *56*, 1445−1457.
(50) Sherman, L. S.; Blum, J. D.; Johnson, K. P.; Keeler, G. J.; Barres, J. A.; Douglas, T. A. Mass-independent fractionation of mercury isotopes in Arctic snow driven by sunlight. *Nat. Geosci* **2010**, *3*, 173−177.
(51) Zhao, H.; Meng, B.; Sun, G.; Lin, C.-J.; Feng, X.; Sommar, J. Chemistry and Isotope Fractionation of Divalent Mercury during Aqueous Reduction Mediated by Selected Oxygenated Organic Ligands. *Environ. Sci. Technol.* **2021**, *55*, 13376 DOI: 10.1021/acs.est.1c03171.
(52) Zhang, H.; Fu, X.; Wu, X.; Deng, Q.; Tang, K.; Zhang, L.; Sommar, J.; Sun, G.; Feng, X. Using Mercury Stable Isotopes to Quantify Bidirectional Water−Atmosphere Hg(0) Exchange Fluxes and Explore Controlling Factors. *Environ. Sci. Technol.* **2023**, *57*, 10673−10685.
(53) Motta, L. C.; Kritee, K.; Blum, J. D.; Tsui, M. T. K.; Reinfelder, J. R. Mercury Isotope Fractionation during the Photochemical Reduction of Hg(II) Coordinated with Organic Ligands. *J. Phys. Chem. A* **2020**, *124*, 2842−2853.
(54) Motta, L. C.; Chien, A. D.; Rask, A. E.; Zimmerman, P. M. Mercury Magnetic Isotope Effect: A Plausible Photochemical Mechanism. *J. Phys. Chem. A* **2020**, *124*, 3711−3719.
(55) Douglas, T. A.; Blum, J. D. Mercury Isotopes Reveal Atmospheric Gaseous Mercury Deposition Directly to the Arctic Coastal Snowpack. *Environmental Science & Technology Letters* **2019**, *6*, 235−242.
(56) Sonke, J. E. A global model of mass independent mercury stable isotope fractionation. *Geochim. Cosmochim. Acta* **2011**, *75*, 4577−4590.
(57) Schmidt, J. A.; Jacob, D. J.; Horowitz, H. M.; Hu, L.; Sherwen, T.; Evans, M. J.; Liang, Q.; Suleiman, R. M.; Oram, D. E.; Le Breton, M.; Percival, C. J.; Wang, S.; Dix, B.; Volkamer, R. Modeling the observed tropospheric BrO background: Importance of multiphase chemistry and implications for ozone, OH, and mercury. *J. Geophys Res-Atmos* **2016**, *121*, 11819−11835.
(58) Dibble, T. S.; Tetu, H. L.; Jiao, Y.; Thackray, C. P.; Jacob, D. J. Modeling the OH-Initiated Oxidation of Mercury in the Global Atmosphere without Violating Physical Laws. *J. Phys. Chem. A* **2020**, *124*, 444−453.
(59) Wang, X.; Jacob, D. J.; Downs, W.; Zhai, S.; Zhu, L.; Shah, V.; Holmes, C. D.; Sherwen, T.; Alexander, B.; Evans, M. J.; Eastham, S. D.; Neuman, J. A.; Veres, P. R.; Koenig, T. K.; Volkamer, R.; Huey, L. G.; Bannan, T. J.; Percival, C. J.; Lee, B. H.; Thornton, J. A. Global tropospheric halogen (Cl, Br, I) chemistry and its impact on oxidants. *Atmospheric Chemistry and Physics* **2021**, *21*, 13973−13996.
(60) Zheng, W.; Chandan, P.; Steffen, A.; Stupple, G.; De Vera, J.; Mitchell, C. P. J.; Wania, F.; Bergquist, B. A. Mercury stable isotopes reveal the sources and transformations of atmospheric Hg in the high Arctic. *Appl. Geochem.* **2021**, *131*, No. 105002.
(61) Qiu, Y.; Gai, P. X.; Yue, F. E.; Zhang, Y. Y.; He, P. Z.; Kang, H.; Yu, X. W.; Lam, P. K. S.; Chen, J. B.; Xie, Z. Q. Identification of potential sources of elevated PM2.5-Hg using mercury isotopes during haze events. *Atmos. Environ.* **2021**, *247*, No. 118203.
(62) Li, C. J.; Chen, J. B.; Angot, H.; Zheng, W.; Shi, G. T.; Ding, M. H.; Du, Z. H.; Zhang, Q. G.; Ma, X. Y.; Kang, S. C.; Xiao, C. D.; Ren, J. W.; Qin, D. H. Seasonal Variation of Mercury and Its Isotopes in Atmospheric Particles at the Coastal Zhongshan Station, Eastern Antarctica. *Environ. Sci. Technol.* **2020**, *54*, 11344−11355.
(63) Xu, H.; Sonke, J. E.; Guinot, B.; Fu, X.; Sun, R.; Lanzanova, A.; Candaudap, F.; Shen, Z.; Cao, J. Seasonal and Annual Variations in Atmospheric Hg and Pb Isotopes in Xi'an. *China; Environmental science & technology* **2017**, *51*, 3759−3766.
(64) Fu, X.; Zhang, H.; Feng, X.; Tan, Q.; Ming, L.; Liu, C.; Zhang, L. Domestic and Transboundary Sources of Atmospheric Particulate Bound Mercury in Remote Areas of China: Evidence from Mercury Isotopes. *Environ. Sci. Technol.* **2019**, *53*, 1947−1957.
(65) Jiskra, M.; Heimbürger-Boavida, L.-E.; Desgranges, M.-M.; Petrova, M. V.; Dufour, A.; Ferreira-Araujo, B.; Masbou, J.; Chmeleff, J.; Thyssen, M.; Point, D.; Sonke, J. E. Mercury stable isotopes constrain atmospheric sources to the ocean. *Nature* **2021**, *597*, 678−682.
(66) Kurz, A. Y.; Blum, J. D.; Johnson, M. W.; Nadelhoffer, K.; Zak, D. R. Isotopic composition of mercury deposited via snow into mid-latitude ecosystems. *Sci. Total Environ.* **2021**, *784*, No. 147252.
(67) Fu, X.; Liu, C.; Zhang, H.; Xu, Y.; Zhang, H.; Li, J.; Lyu, X.; Zhang, G.; Guo, H.; Wang, X.; Zhang, L.; Feng, X. Isotopic compositions of atmospheric total gaseous mercury in 10 Chinese cities and implications for land surface emissions. *Atmospheric Chemistry and Physics* **2021**, *21*, 6721−6734.
(68) Fu, X.; Yang, X.; Tan, Q.; Ming, L.; Lin, T.; Lin, C.-J.; Li, X.; Feng, X. Isotopic Composition of Gaseous Elemental Mercury in the Marine Boundary Layer of East China Sea. *Journal of Geophysical Research: Atmospheres* **2018**, *123*, 7656−7669.
(69) Huang, Q.; Chen, J.; Huang, W.; Fu, P.; Guinot, B.; Feng, X.; Shang, L.; Wang, Z.; Wang, Z.; Yuan, S.; Cai, H.; Wei, L.; Yu, B. Isotopic composition for source identification of mercury in atmospheric fine particles. *Atmospheric Chemistry and Physics* **2016**, *16*, 11773−11786.
(70) Das, R.; Wang, X.; Khezri, B.; Webster, R. D.; Sikdar, P. K.; Datta, S.; Blum, J. D.; Hintelmann, H. Mercury isotopes of atmospheric particle bound mercury for source apportionment study in urban Kolkata, India. *Elementa: Sci. Anthropocene* **2016**, *4*, 1−12, DOI: 10.12952/journal.elementa.000098.
(71) Guo, J.; Tripathee, L.; Kang, S.; Zhang, Q.; Huang, J.; Mani Sharma, C.; Chen, P.; Paudyal, R.; Rupakheti, D. Atmospheric particle-bound mercury in the northern Indo-Gangetic Plain region: Insights into sources from mercury isotope analysis and influencing factors. *Geosci. Front.* **2022**, *13*, No. 101274.
(72) Sun, L.; Zhang, X.; Zheng, J.; Zheng, Y.; Yuan, D.; Chen, W., Mercury concentration and isotopic composition on different atmospheric particles (PM10 and PM2.5) in the subtropical coastal suburb of Xiamen Bay, Southern China; Atmospheric Environment, 2021, 261. DOI: 10.1016/j.atmosenv.2021.118604.
(73) Xu, H. M.; Sun, R. Y.; Cao, J. J.; Huang, R.-J.; Guinot, B.; Shen, Z. X.; Jiskra, M.; Li, C. X.; Du, B. Y.; He, C.; Liu, S. X.; Zhang, T.; Sonke, J. E. Mercury stable isotope compositions of Chinese urban

https://doi.org/10.1021/acs.est.4c02600
Environ. Sci. Technol. XXXX, XXX, XXX−XXX

fine particulates in winter haze days: Implications for Hg sources and transformations. *Chem. Geol.* **2019**, *504*, 267−275.
(74) Rolison, J. M.; Landing, W. M.; Luke, W.; Cohen, M.; Salters, V. J. M. Isotopic composition of species-specific atmospheric Hg in a coastal environment. *Chem. Geol.* **2013**, *336*, 37−49.
(75) Huang, Q.; Reinfelder, J. R.; Fu, P.; Huang, W. Variation in the mercury concentration and stable isotope composition of atmospheric total suspended particles in Beijing. *China; Journal of hazardous materials* **2020**, *383*, No. 121131.
(76) Saiz-Lopez, A., Bromine oxide in the mid-latitude marine boundary layer; *Geophys. Res. Lett.*, **2004**, *31*. DOI: 10.1029/2003gl018956.
(77) Zhu, L.; Jacob, D. J.; Eastham, S. D.; Sulprizio, M. P.; Wang, X.; Sherwen, T.; Evans, M. J.; Chen, Q.; Alexander, B.; Koenig, T. K.; Volkamer, R.; Huey, L. G.; Le Breton, M.; Bannan, T. J.; Percival, C. J. Effect of sea salt aerosol on tropospheric bromine chemistry. *Atmospheric Chemistry and Physics* **2019**, *19*, 6497−6507.
(78) UN-Environment, Global Mercury Assessment 2018. UN Environment Programme, Chemicals and Health Branch, Geneva, Switzerlan; 2019.
(79) Zhang, Y.; Zhang, P.; Song, Z.; Huang, S.; Yuan, T.; Wu, P.; Shah, V.; Liu, M.; Chen, L.; Wang, X.; Zhou, J.; Agnan, Y. An updated global mercury budget from a coupled atmosphere-land-ocean model: 40% more re-emissions buffer the effect of primary emission reductions. *One Earth* **2023**, *6*, 316−325.
(80) Selin, N. E.; Jacob, D. J.; Park, R. J.; Yantosca, R. M.; Strode, S.; Jaeglé, L.; Jaffe, D. Chemical cycling and deposition of atmospheric mercury: Global constraints from observations. *Journal of Geophysical Research* **2007**, *112*, 112.
(81) Pal, B.; Ariya, P. Gas-phase HO-initiated reactions of elemental mercury: kinetics, product studies, and atmospheric implications. *Environ. Sci. Technol.* **2004**, *38*, 5555−5566.
(82) IPCC, Climate change: The physical science basis. The Fifth Assessment Report, 5, 1552.; 2013.
(83) Wang, Y.; Wu, P.; Zhang, Y. Climate-driven changes of global marine mercury cycles in 2100. *Proc. Natl. Acad. Sci. U. S. A.* **2023**, *120*, No. e2202488120.
(84) Orr, J. C.; Fabry, V. J.; Aumont, O.; Bopp, L.; Doney, S. C.; Feely, R. A.; Gnanadesikan, A.; Gruber, N.; Ishida, A.; Joos, F.; Key, R. M.; Lindsay, K.; Maier-Reimer, E.; Matear, R.; Monfray, P.; Mouchet, A.; Najjar, R. G.; Plattner, G. K.; Rodgers, K. B.; Sabine, C. L.; Sarmiento, J. L.; Schlitzer, R.; Slater, R. D.; Totterdell, I. J.; Weirig, M. F.; Yamanaka, Y.; Yool, A. Anthropogenic ocean acidification over the twenty-first century and its impact on calcifying organisms. *Nature* **2005**, *437*, 681−686.
(85) Sinha, E.; Michalak, A. M.; Balaji, V. Eutrophication will increase during the 21st century as a result of precipitation changes. *Science* **2017**, *357*, 405−408.
(86) Kessouri, F.; McWilliams, J. C.; Bianchi, D.; Sutula, M.; Renault, L.; Deutsch, C.; Feely, R. A.; McLaughlin, K.; Ho, M.; Howard, E. M.; Bednaršek, N.; Damien, P.; Molemaker, J.; Weisberg, S. B., Coastal eutrophication drives acidification, oxygen loss, and ecosystem change in a major oceanic upwelling system; *Proc. Natl. Acad. Sci. U. S. A.*, **2021**, *118*. DOI: 10.1073/pnas.2018856118.

https://doi.org/10.1021/acs.est.4c02600
Environ. Sci. Technol. XXXX, XXX, XXX−XXX